1 **Simultaneous electrochemical determination of furazolidone and dimetridazole**

2 **using transition metal titanates with ilmenite type structure**

3 Jesu Amalraj Antolin Jesila[a], Narasimha Murthy Umesh[a], Sea-Fue Wang[a, *]

4 [a]Department of Materials and Mineral Resources Engineering, National Taipei University of Technology, No. 1,

5 Section 3, Chung-Hsiao East Road, Taipei 106, Taiwan, ROC

6 *Corresponding author – Sea-Fue Wang

7 Email: *sfwang@ntut.edu.tw*

8

Materials and apparatus

9 **Materials and apparatus**

10   Cobalt nitrate hexahydrate ($CoNO_3.6H_2O$), nickel nitrate hexahydrate ($NiNO_3.6H_2O$), zinc

11 nitrate hexahydrate ($ZnNO_3.6H_2O$), nitric acid (HNO_3), sodium hydroxide (NaOH), ethylene

12 glycol, tetrabutyl titanate (Ti precursor) are bought from Sigma-Aldrich, Canada. Every single

13 substance and organic chemicals were purchased from Sigma-Aldrich, Taiwan, and utilized

14 moving forward without any more sanitization. Using double-distilled de-ionized water (DD), all

15 needed solutions were prepared, and also as a supporting electrolyte, Na_2HPO_4 (disodium

16 hydrogen phosphate) and NaH_2PO_4 (sodium dihydrogen phosphate) were used. NaOH and HNO_3

17 were used to prepare all the pH buffer solutions.

18 **Instrument**

19   The surface morphology examinations and the elemental analysis of as-prepared metal

20 titanates have been performed using dispersive energy X-ray (EDX, HORIBA EMAX XACT).

21 The crystallographic analysis of our composite has been carried out with X-ray diffraction (XRD)

22 spectroscopy (Rigaku D/maxB, DMX-2200), and transmission electron microscopy (TEM) was

23 analyzed using H-7600, Hitachi-Japan.

Synthesis procedure

In this simple synthesis procedure, 6 mM of the cobalt precursor and 6 mM of Ti^{4+} precursors were added to a mixture of solvents like ethanol and ethylene glycol 75 mL (1:1). The above mixture was stirred for 30 min by using a magnetic stirrer to obtain a homogenous solution. Later the mixed solution was transferred to a Teflon-lined autoclave and maintained at 200 °C for 18 h. Then the autoclave was allowed to cool down generally to room temperature, and the formed product was collected via centrifugation which was washed thoroughly with water and ethanol five times. Then, the precipitate was dried at 60 °C overnight, and finally, the obtained powder was calcined at 700 °C for 2 h with a heating and cooling rate 7 °C/min to achieve the target compound cobalt titanate ($CoTiO_3$). Similarly, instead of Cobalt precursor, nickel nitrate and zinc nitrate were used to synthesize nickel titanate and zinc titanate ($NiTiO_3$ and $ZnTiO_3$).

Mechanism of crystal growth formation

The physical characterization results obtained for metal titanates depict phase and morphology confirmation based on the above-given information. The formation mechanism of perovskite-type metal titanates involving the crystallization process was the same as previously reported literature[1,2]. A possible formation mechanism for the crystallization and polymerization process is shown in **Figure S1**. The mechanism describes the formation of micro/nanostructured metal titanates. A specific volume of ethanol to ethylene glycol was used for the synthesis. Ethylene glycol acts as a complexing agent and plays a vital role in the structural property of as-synthesized metal titanates. To obtain Ti–glycolate polymer with the chelating ring-like structure or chain-like structure, ethylene glycol, a bidentate ligand, may react with tetrabutyl titanate. During the solvothermal process, because of metal ions' coordination ability with ethylene glycol, Ti–O–EG polymer chains involve absorbing M^{2+} (M = Co, Ni, Zn) ions. Ti's stabilization obtained

2

47   by the uniformly dispersed structure–O–EG polymer chains is prolonged by increasing ethanol's

48   volume ratio to ethylene glycol (2:1). Due to ethylene glycol molecules' hydrogen bonding, the

49   polymer chains slowly agglomerate with an additional increase in ethanol volume to ethylene

50   glycol (1:1). The porous structure of metal titanates is obtained by drying and calcination of the

51   received product. The porous structure is obtained due to the decomposition of organic polymers.
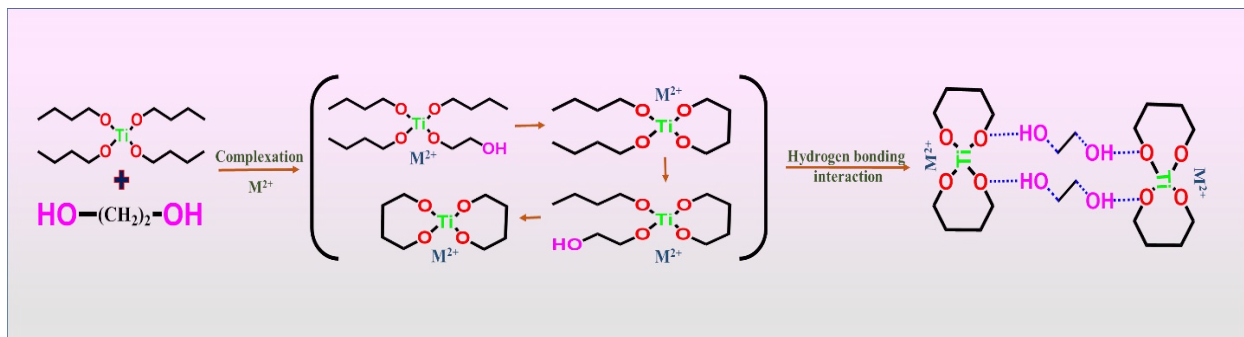
52

53   **Figure S1. Formation mechanism of metal titanate**
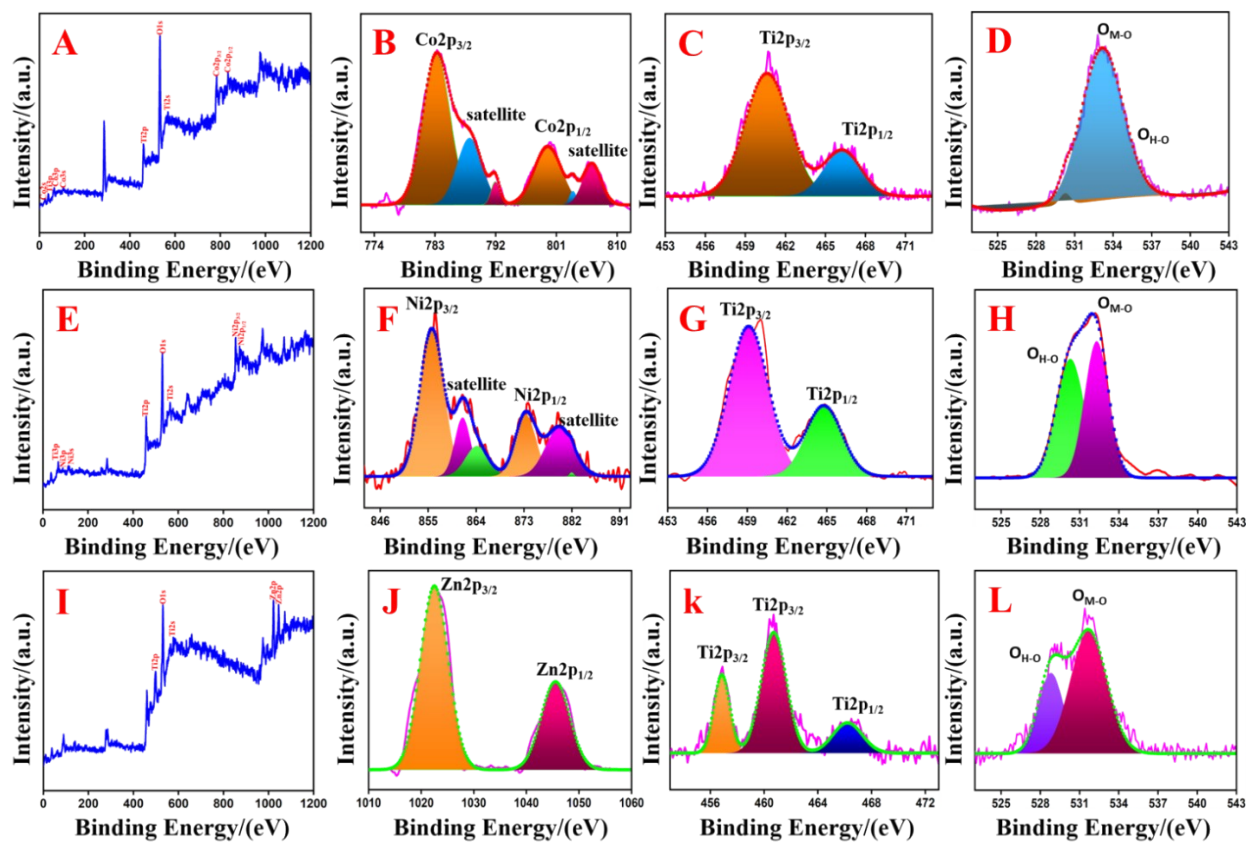
54

55 **Figure S2**. XPS spectra of A- CoTiO$_3$: survey spectrum, B– Co 2p spectra, C– Ti 2p spectra, and

56 D– O 1s spectra. Figure 2E- XPS spectra of NiTiO$_3$: survey spectrum, F– Ni 2p spectra, G– Ti 2p

57 spectra, and H– O 1s spectra. Figure 2I- XPS spectra of ZnTiO$_3$: survey spectrum, J– Zn 2p spectra,

58 K– Ti 2p spectra, and L– O 1s spectra.

59 **Electrochemical instrument**

60   Three electrode system is used to perform electrochemical studies. For the working

61 electrode glassy carbon electrode (GCE), as the counter electrode platinum wire and as the

62 reference electrode, silver/silver chloride (Ag/AgCl in 3M KCl) was used.
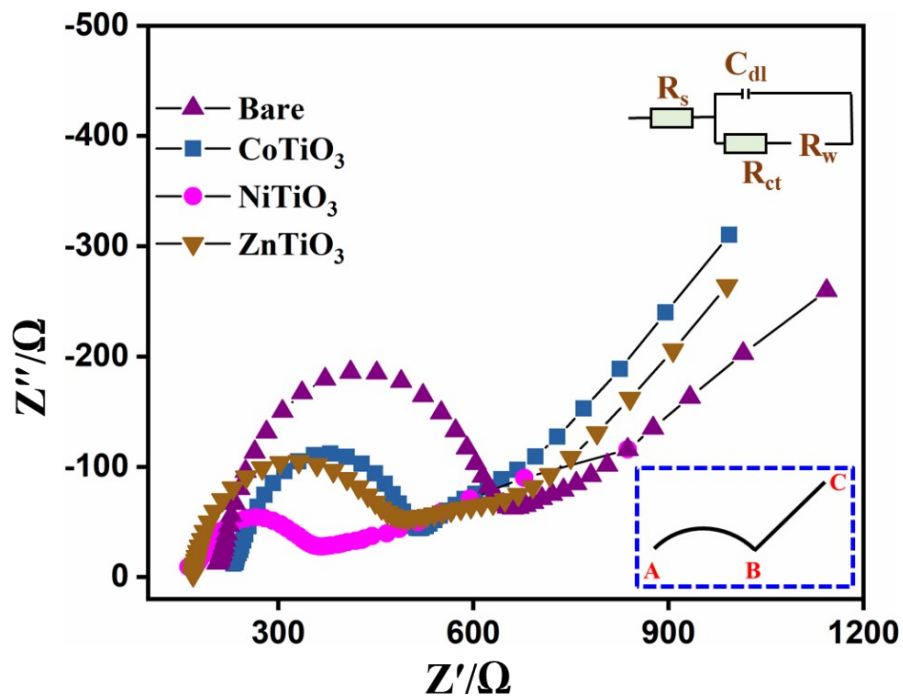
63

64   **Figure S3.** EIS analysis for different modified electrodes.

65

66

67 **Table S1** Parameters related to the Nyquist plot and average size calculation.

Electrode	R_s (Ω)	R_{ct} (Ω)	C_{dl} ($\mu F/cm^2$)	EASA (cm^2)	crystallite size [XRD (nm)]	Average size [TEM (nm)]
Bare GCE	210.78	436.34	1.61	0.1466	-	-
CoTiO$_3$/GCE	235.84	281.2	1.76	0.1850	66.94	93.5
NiTiO$_3$/GCE	167.92	198.64	2.16	0.2218	39.34	70.32
ZnTiO$_3$/GCE	166.67	318.55	1.65	0.1659	86.41	104.78

68
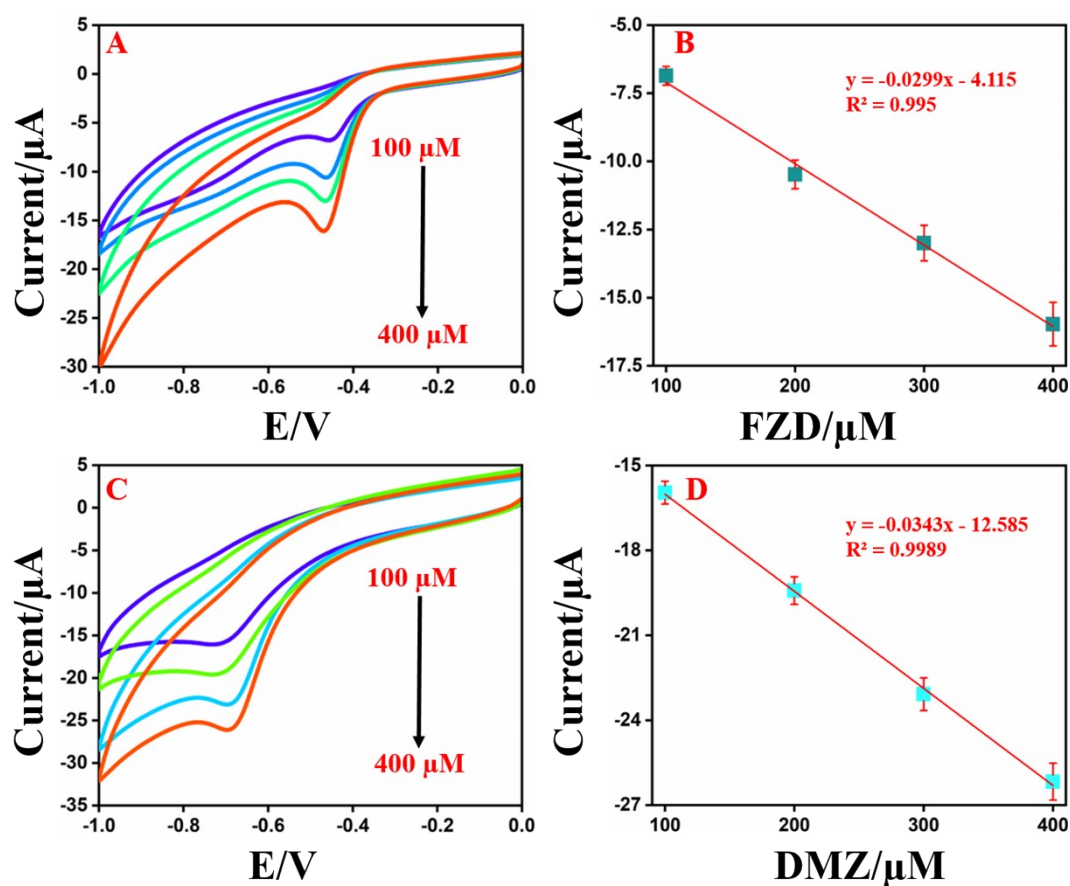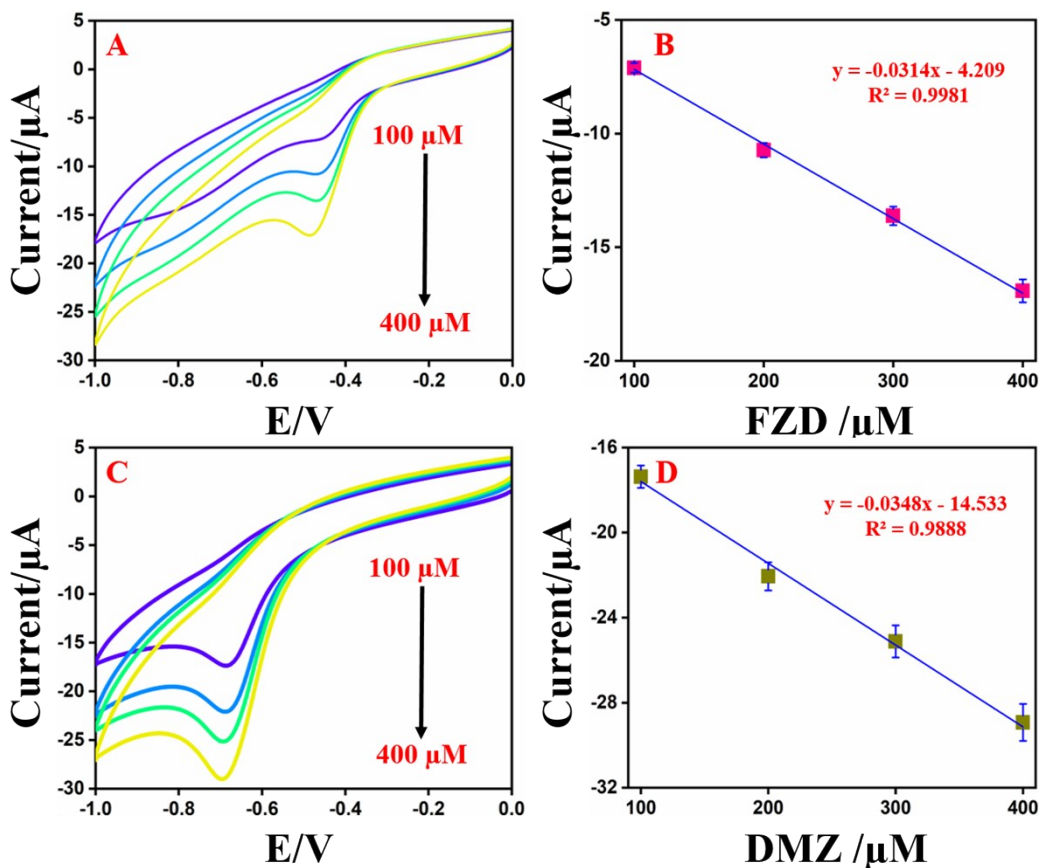

69

70 **Figure S4**. A-Different concentration of FZD (100 to 400 μM) at CoTiO$_3$/GCE in 0.1 M PB

71 solution (pH 7.0) at 50 mV/s, B-calibration plot for the concentration of FZD Vs. current obtained,

72 C- different concentration of DMZ (100 to 400 µM) at CoTiO$_3$/GCE in 0.1 M PB solution (pH

73 7.0) at 50 mV/s, D-calibration plot for the concentration of DMZ Vs. current obtained.

74   **Figure S4** depicts the individual CVs for CoTiO$_3$/GCE with different concentrations

75 of FZD (100 – 400 µM) is shown in **Figure S4.A** and DMZ (100 – 400 µM) are shown in **Figure**

76 **S4.C**. An excellent linear response upon each addition was observed in both FZD and DMZ.

77 **Figure S4.B** depicts the linearity plot for the concentration of FZD vs. current obtained, and

78 **Figure S4.D** displays the linearity plot for the concentration of DMZ vs. current obtained. In both,

79 the plot concentration of each analyte is directly proportional to the current obtained.

80

81

82   **Figure S5**. A-Different concentration of FZD (100 to 400 µM) at NiTiO$_3$/GCE in 0.1 M PB

83   solution (pH 7.0) at 50 mV/s, B-calibration plot for the concentration of FZD Vs. current obtained,

84   C- different concentration of DMZ (100 to 400 µM) at NiTiO$_3$/GCE in 0.1 M PB solution (pH 7.0)

85   at 50 mV/s, D-calibration plot for the concentration of DMZ Vs. current obtained.

86   Secondly, **Figure S5** depicts the individual CVs for NiTiO$_3$/GCE with different concentrations of

87   FZD (100 – 400 µM) is shown in **Figure S5.A** and DMZ (100 – 400 µM) are shown in **Figure**

88   **S5.C**. An excellent linear response upon each addition was observed in both FZD and DMZ.

89   **Figure S5.B** depicts the linearity plot for the concentration of FZD vs. current obtained, and

90   **Figure S5.D** displays the linearity plot for the concentration of DMZ vs. current obtained. In both,

91   the plot concentration of each analyte is directly proportional to the current obtained.

92
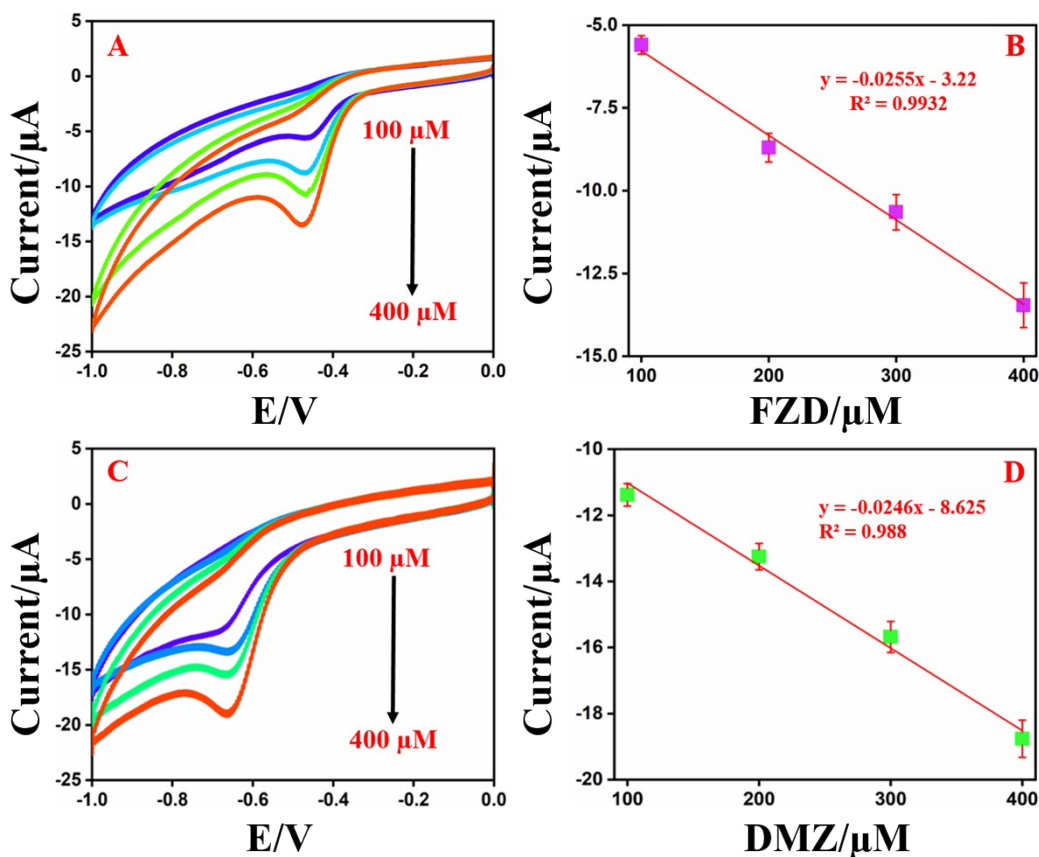
93

94 **Figure S6**. A-Different concentration of FZD (100 to 400 µM) at $ZnTiO_3$/GCE in 0.1 M PB

95 solution (pH 7.0) at 50 mV/s, B-calibration plot for the concentration of FZD Vs. current obtained,

96 C- different concentration of DMZ (100 to 400 µM) at $ZnTiO_3$/GCE in 0.1 M PB solution (pH

97 7.0) at 50 mV/s, D-calibration plot for the concentration of DMZ Vs. current obtained.

98   Finally, **Figure S6** depicts the individual CVs for $ZnTiO_3$/GCE with different

99 concentrations of FZD (100 – 400 µM) shown in **Figure S6.A** and DMZ (100 – 400 µM) shown

100 in **Figure S6.C**. An excellent linear response upon each addition was observed in both FZD and

101 DMZ. **Figure S6.B** depicts the linear calibration plot for the concentration of FZD *vs.* current

102 obtained, and **Figure S6.D** displays the linear calibration plot for the concentration of DMZ *vs.*

103 current obtained. In both, the plot concentration of each analyte is directly proportional to the

104 current obtained. Besides, the individual current response received at each modified electrode for

105 FZD and DMZ as shown in **Figure S6**.
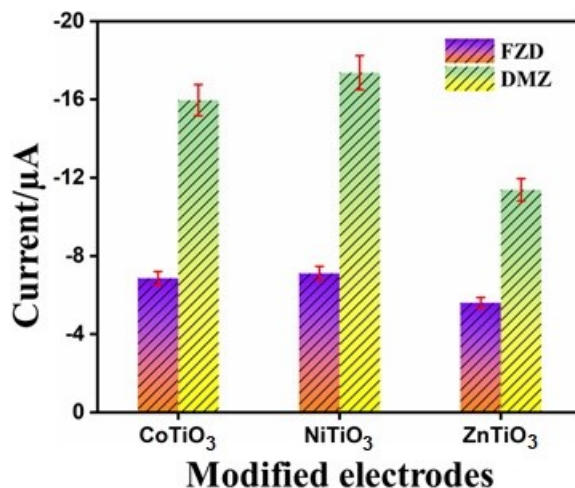
106

107 **Figure S7**. Bar diagram for different metal titanate modified electrodes of individual concentration

108 of FZD and DMZ *vs.* current obtained.

109 The above Figure demonstrates that $NiTiO_3$/GCE showed an outstanding sensing performance and

110 anti-fouling effects of individual analytes such as FZD and DMZ than $CoTiO_3$/GCE and

111 ZnTiO$_3$/GCE. The reason might be due to the highly selective sensing capability of FZD and DMZ

112 at the NiTiO$_3$ electrode surface, more significant electrochemical active sites, and larger

113 electrochemical active surface area.

114
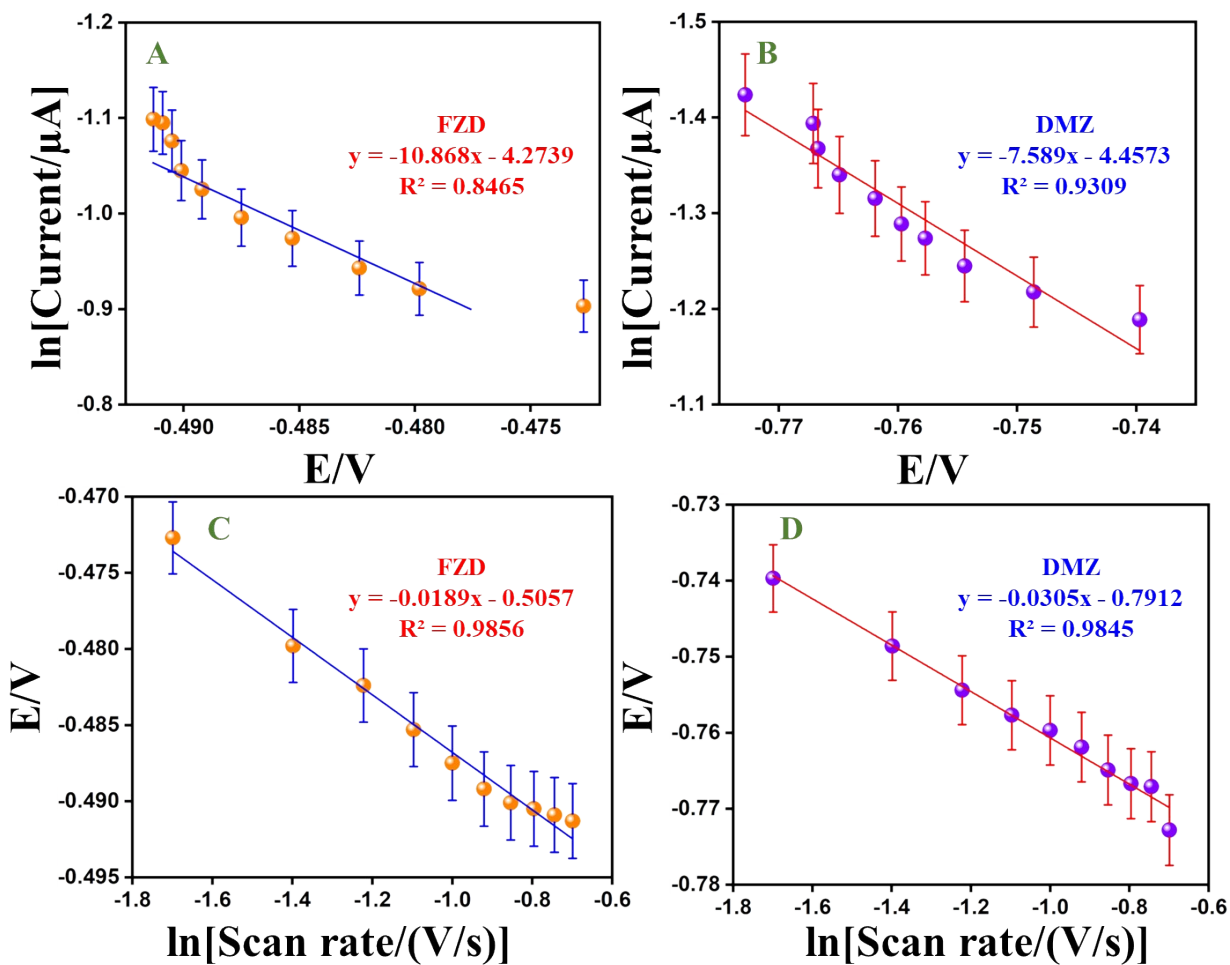
115

116 **Figure S8**. Corresponding calibration plot of Potential (E/V) *vs*. ln. Current (µA) A. for FZD and

117 B. for DMZ in 0.1 M PB solution (pH 7.0) at NiTiO$_3$/GCE towards the simultaneous detection of

118 100 µM FZD and DMZ. Corresponding calibration plot of ln. Scan rate (V/s) *vs*. Potential (E/V)

119 A. for FZD and B. for DMZ in 0.1 M PB solution (pH 7.0) at NiTiO$_3$/GCE towards the

120 simultaneous detection of 100 µM FZD and DMZ

121 **Table S2** Electro-catalytic and kinetic Parameters.

Analytes	surface coverage (Γ) nM/cm^2	No. of electrons transferred	Charge transfer coefficient (α)	Rate constant (Ks) s^{-1}
FZD	1.8127	3.95	0.8385	6.5805
DMZ	3.5118	4.06	0.8872	3.9813

122
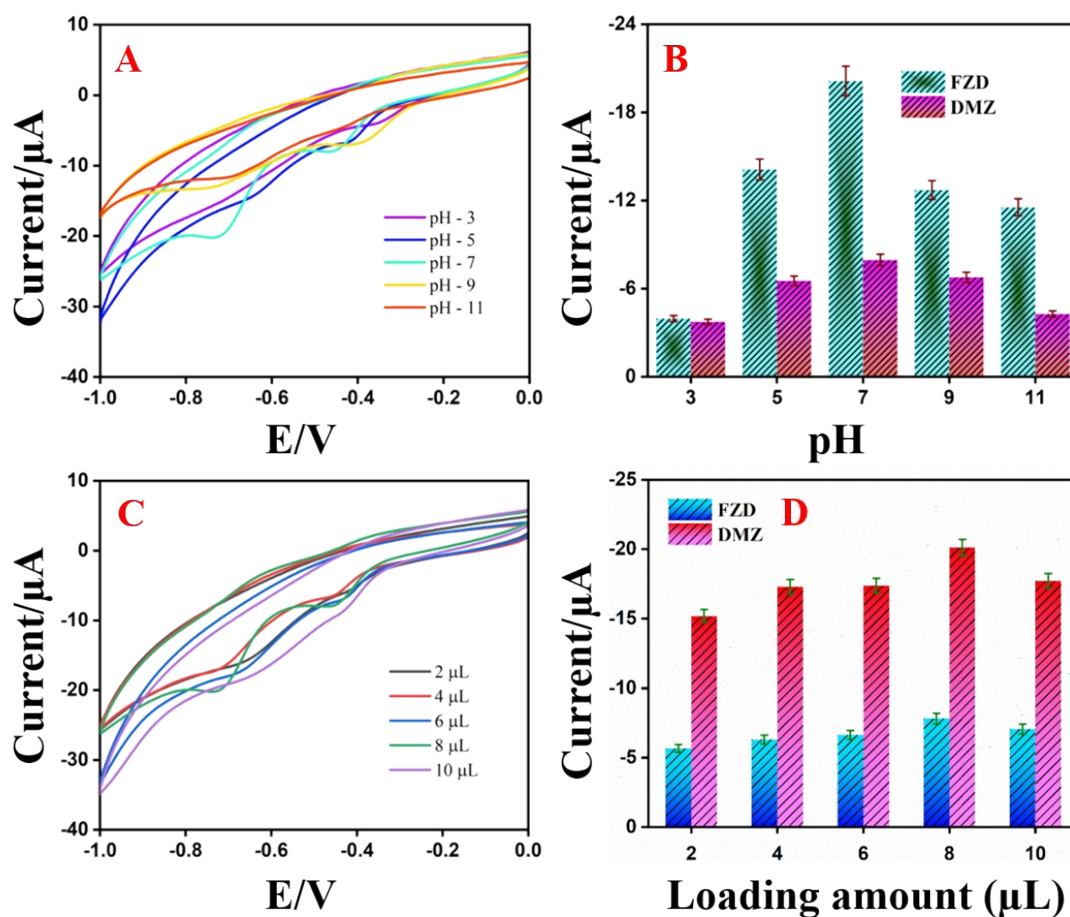
123

124 **Figure S9**. A-CV's for the effect of pH on NiTiO$_3$/GCE towards 150 μM simultaneous addition

125 of FZD and DMZ at 50 mV/s, B-bar diagram for different pH *vs*. Current, C-CV's for the effect

126 of different loading amount in NiTiO$_3$/GCE in 0.1 M PB solution (pH 7.0) at 50 mV/s 150

127 µM simultaneous addition of FZD and DMZ and D-bar diagram for loading amount *vs.* Current

128 obtained.

**Optimization of DPV for the quantification of FZD and DMZ:**

130   Using the modified simplex method, the variables related to the DPV technique were

131 optimized to maximize the cathodic current related to FZD and DMZ reduction. The optimization

132 was undertaken in such a manner that one parameter was always altered within the procedure while

133 the second one was remained unchanged.[3,4] For this DPV optimization, the experiment was

134 performed with FZD (40 µM) and DMZ (60 µM) in 0.1 M PB solution (pH 7.0) at the potential

135 range of -0.2 V to -1.2 V respectively. The experiments were performed until achieving the

136 optimum parameters in both the reduction of FZD and DMZ individually, and the optimized

137 conditions are shown in Table S3.

138   **Table S3** Optimized parameters for FZD and DMZ analysis by DPV.

| Parameters	Optimized values
Increment Potential (mV)	4
Pulse Amplitude (mV)	50
Pulse Width (ms)	50
Pulse Period (ms)	300
Sampling width (ms)	16.7
Quiet time (s)	1

139

140
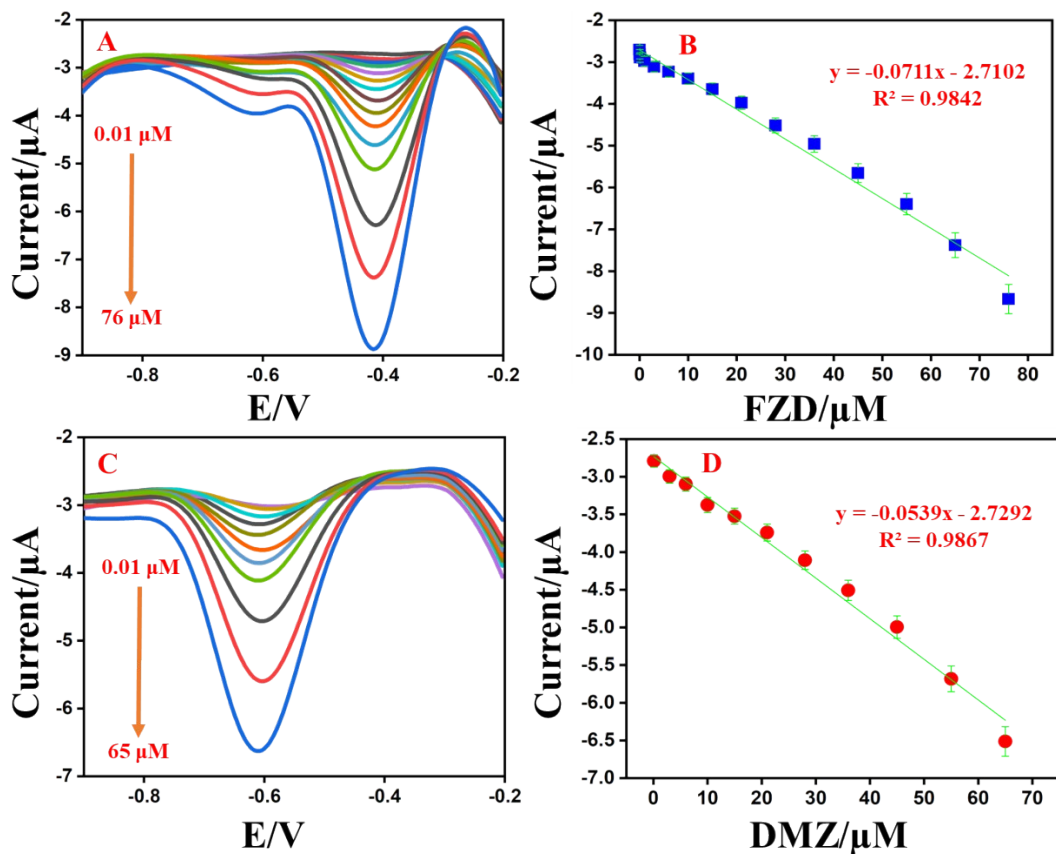
Figure S10. A– Individual DPV analysis of FZD (0.01 to 76 µM) at NiTiO₃/GCE in 0.1 M PB solution (pH 7.0) at the potential range of -0.2 V to -1.2 V with the optimized parameters (pulse amplitude – 50 mV; pulse width – 50 ms; pulse period – 300 ms; quiet time – 1 s), B– Calibration plot of concentration of FZD *vs*. current, C– Individual DPV analysis of DMZ (0.01 to 65 µM) at NiTiO₃/GCE in 0.1 M PB solution (pH 7.0) at the potential range of -0.2 V to -1.2 V with the optimized parameters (pulse amplitude – 50 mV; pulse width – 50 ms; pulse period – 300 ms; quiet time – 1 s), D– Calibration plot of concentration of DMZ Vs current.
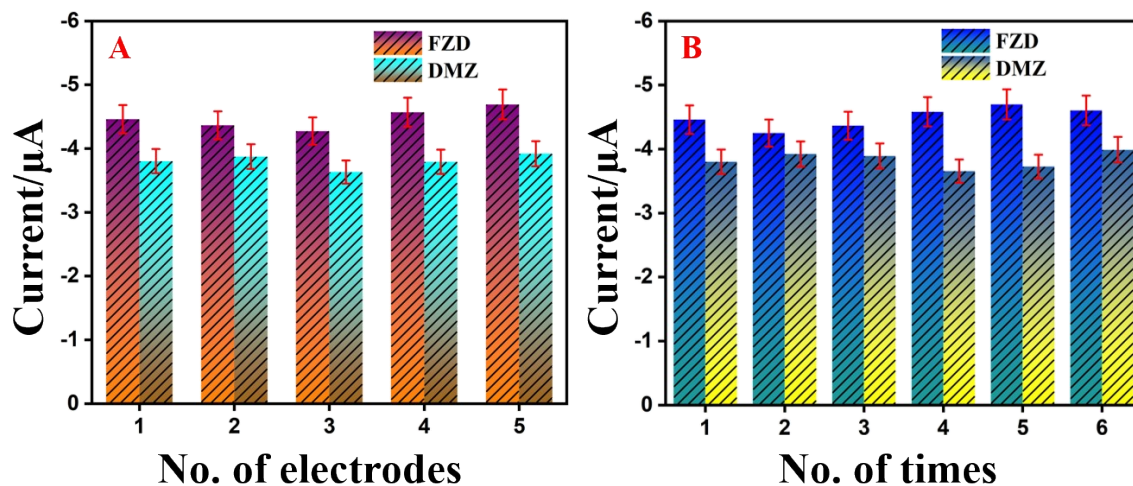
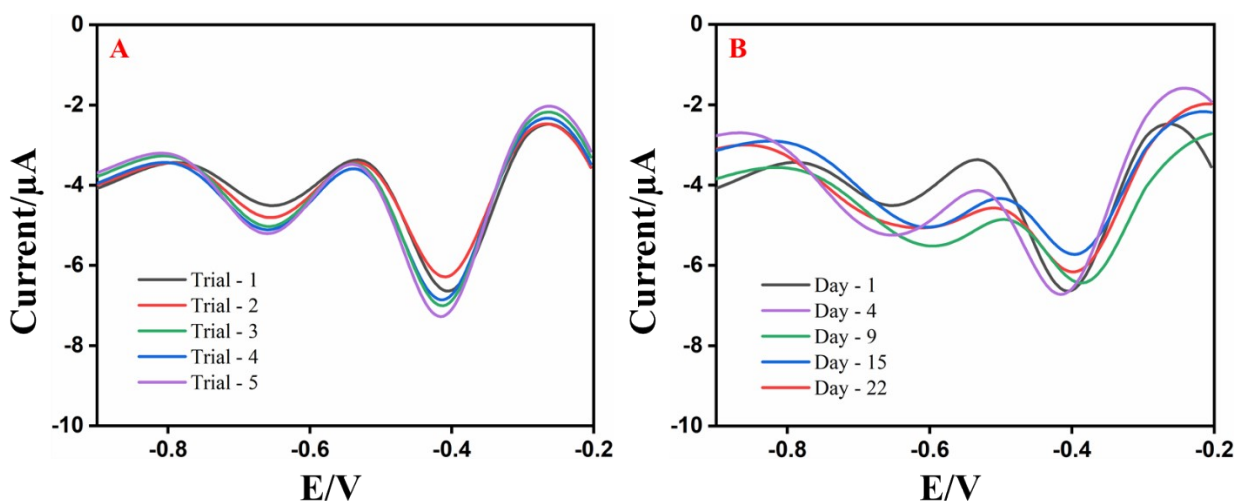**Figure S11**. A-Reproducubility and B-repeatability studies of NiTiO$_3$/GCE towards 150 μM simultaneous addition of FZD and DMZ at 50 mV/s in 0.1 M PB solution (pH 7.0)

Figure S12. A&B – Intra-day stability analysis and Inter-day stability analysis with 50 μM of FZD and DMZ at NiTiO$_3$/GCE in 0.1 M PB solution (pH 7.0) at the potential range of -0.2 V to -1.2 V with the optimized parameters (pulse amplitude – 50 mV; pulse width – 50 ms; pulse period – 300 ms; quiet time – 1 s).

162 **References**

163 1   A. Moghtada and R. Ashiri, *Ultrason. Sonochem.*, 2015, **26**, 293–304.

164 2   A. Moghtada and R. Ashiri, *Ultrason. Sonochem.*, 2016, **33**, 141–149.

165 3   G. Y. Aguilar-Lira, A. Rojas-Hernández, J. A. Rodriguez, M. E. Páez-Hernández and G.

166   A. Álvarez-Romero, *J. Electrochem. Soc.*, 2020, **167**, 166510.

167 4   Ľ. Švorc, K. Borovska, K. Cinková, D. M. Stanković and A. Planková, *Electrochim. Acta*,

168   2017, **251**, 621–630.

169